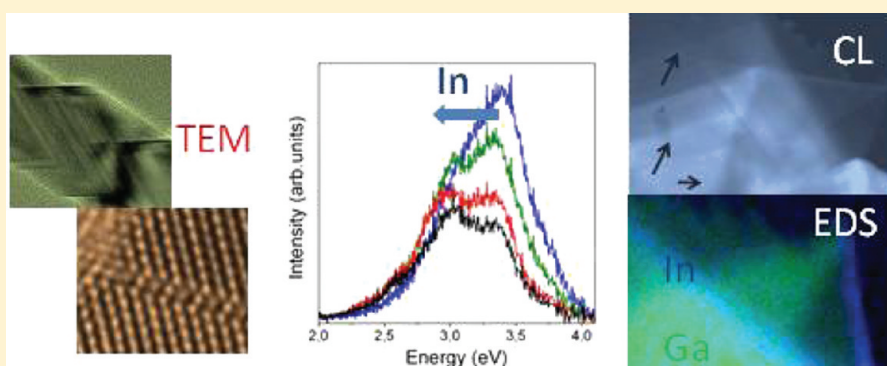# In-Doped Gallium Oxide Micro- and Nanostructures: Morphology, Structure, and Luminescence Properties

Iñaki López, Antonio D. Utrilla, Emilio Nogales, Bianchi Méndez,* and Javier Piqueras

Departamento de Física de Materiales, Facultad de Ciencias Físicas, Universidad Complutense de Madrid, 28040 Madrid, Spain

Andrea Peche, J. Ramírez-Castellanos, and Jose M. González-Calbet

Departamento de Química Inorgánica, Facultad de Ciencias Químicas, Universidad Complutense de Madrid, 28040 Madrid, Spain

ABSTRACT: The influence of indium doping on morphology, structural, and luminescence properties of gallium oxide micro- and nanostructures is reported. Indium-doped gallium oxide micro- and nanostructures have been grown by thermal oxidation of metallic gallium in the presence of indium oxide. The dominant morphologies are beltlike structures, which in many cases are twisted leading to springlike structures, showing that In diffusion in Ga_2O_3 influences the microstructure shapes. High-resolution transmission electron microscopy has revealed the presence of twins in the belts, and energy-dispersive X-ray spectroscopy in the scanning electron microscopy (SEM) has detected a segregation of indium impurities at the edges of planar structures. These results suggest that indium plays a major role in the observed morphologies and support the assumption of a layer by layer model as growth mechanism. An additional assessment of indium influence on the defect structure has been performed by cathodoluminescence in the SEM, X-ray photoelectron microscopy, and spatially resolved Raman spectroscopy.

Trends in fabrication of nanodevices point to novel architectures, which use nanomaterials as building blocks. In this framework, transparent conductive oxide (TCO) nanostructures are considered as candidates to be incorporated into future electronic and optoelectronic nanodevices. The key factor for device applications of these oxides relies on the presence of oxygen vacancies and their interaction with dopants or alloying impurities.[1,2] Among TCOs, monoclinic β-Ga_2O_3 is one of the widest band gap semiconductor oxides (4.9 eV) with n-type conductivity related to donor centers involving oxygen vacancies and/or impurities.[3-5] Ga_2O_3 may be alloyed with other TCOs and be turned into ternary oxide material, in a similar way as indium tin oxide (ITO), which is widely used as a transparent electrode, among other applications. Recently, InGaO thin films have been proposed as channel layers in thin film transistors (TFT), and the influence of growth conditions of oxide films on their electrical properties has been studied.[6] The results in that work show that a decrease in the oxygen partial pressure during films preparation leads to an increase in the channel mobility, and variations in indium concentration influence the mobility and the turn on voltage of the TFT.[6]

Therefore, the addition of doping impurities and the specific growth conditions will influence the functionality of the obtained nano- and microstructures. Thermal evaporation of powders and deposition on a substrate containing catalyst particles is one of the most reported methods to grow nanowires, nanobelts, or more complex morphologies based in ZnO, SnO_2, In_2O_3, or Ga_2O_3 oxides.[7] In our group, a thermal evaporation catalyst-free method has been developed, and several morphologies of interest for optoelectronic and sensing devices have been obtained and characterized.[8-10] In particular, our previous works have demonstrated a tunable luminescence of doped Ga_2O_3 nanowires by the addition of cations, such as Cr, Er, Eu, and Gd ions, and light emission from UV to infrared has been achieved from doped Ga_2O_3 nanowires at room temperature.[9,10] Alternatively, Si and Sn impurities in Ga_2O_3 thin films have been proposed to increase the carrier density
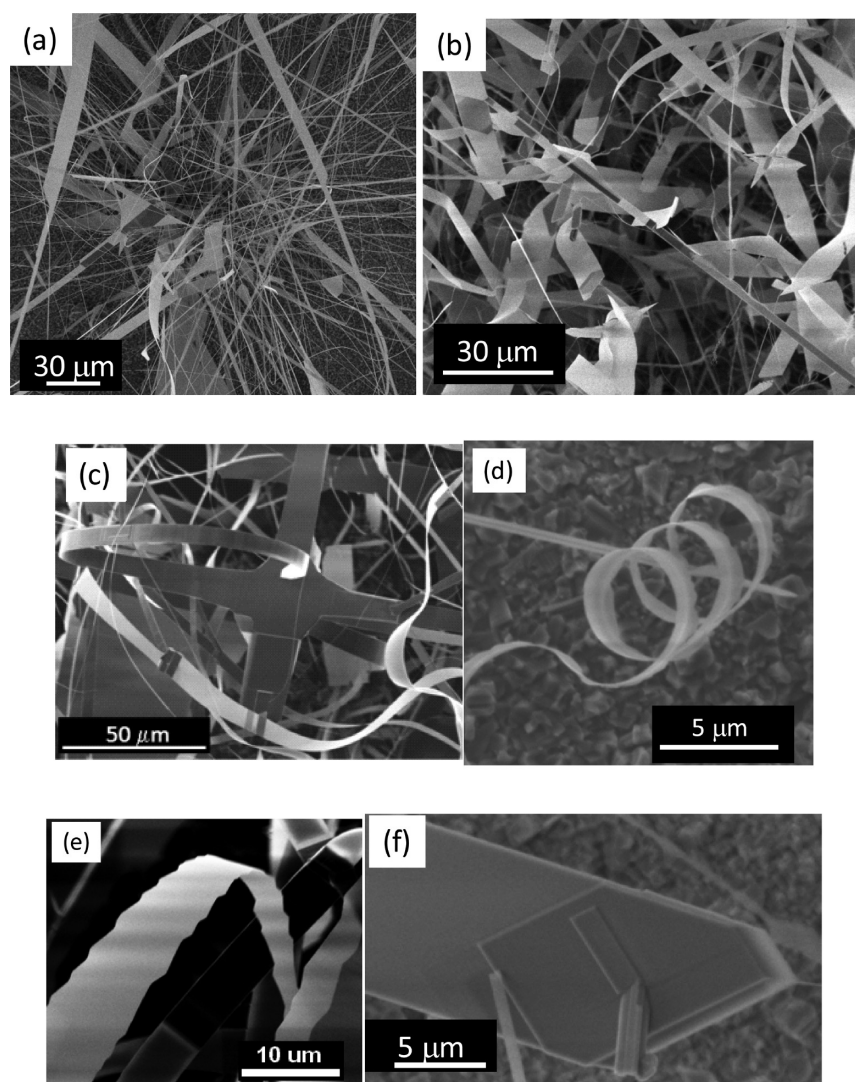
Figure 1. (a) Representative SEM image of undoped Ga_2O_3 microstructures. (b−f) SEM images of In-doped Ga_2O_3 micro- and nanostructures.

and the electrical conductivity.[5,11] In all cases, achieving an effective n-type doping of nanostructures with effective incorporation of impurities in the cationic lattice present difficulties because of out-diffusion processes, which often take place.

In this work, the incorporation of indium atoms in Ga_2O_3 micro- and nanostructures and the relationship between chemical composition, morphology, and optical properties have been investigated. Indium-doped Ga_2O_3 nanoribbons and microstructures have been obtained by controlled thermal annealing of metallic gallium in the presence of indium oxide powders under argon flow. The structure and properties of the obtained micro- and nanostructures have been investigated by means of X-ray diffraction (XRD), scanning and high-resolution transmission electron microscopy (SEM and HRTEM), cathodoluminescence (CL) in the SEM, energy dispersive X-ray spectroscopy (EDS), spatially resolved X-ray photoelectron spectroscopy (XPS), and spatially resolved Raman spectroscopy in a confocal microscope. The high spatial resolution of the employed techniques (XPS, CL, and X-ray microanalysis in the SEM and confocal Raman) enabled to investigate the defects and the indium homogeneity in the obtained structures.

In-doped Ga_2O_3 micro- and nanostructures have been obtained by a thermal evaporation method on compacted gallium oxide pellets. The growth mechanism is based on a vapor−solid (VS) process without the aid of any foreign catalyst. Metallic gallium and indium oxide powders were used as precursor materials, and after a two-step thermal treatment at 1150 °C for 3 h plus 5 h at 1250 °C, a high amount of micro- and nanostructures are formed on the pellet surface. The used temperatures are determined by the oxidation process of the gallium source and subsequent formation of nanowires, as explained elsewhere.[12,13] After the growth process, the structures were placed onto silicon wafer substrates to be characterized. The structural characterization has been carried out by X-ray diffraction (XRD) and TEM. Powder XRD patterns were collected using Cu Kα monochromatic radiation (λ = 1.54056 Å) at room temperature on a Panalytical X'PERT PRO MPD diffractometer equipped with a germanium 111 primary beam monochromator and X'Celerator fast detector. Selected area electron diffraction (SAED) and HRTEM were performed in a JEOL 3000 FEG electron microscope, fitted with a double tilting goniometry stage (±22°, ± 22°). Simulated HRTEM images were calculated by the multislice method using the MacTempas software package. Morphology,

chemical microanalysis, and luminescence have been performed in the same SEM Leica instrument, in which EDS and CL modes were implemented. The study of the structures was complemented with the aid of high resolution photoemission spectra and imaging, performed at the Sincrotrone Elettra Trieste facility (ESCA microscopy line) and Raman spectroscopy in a Horiba Jobin Ybon LabRam HR800 confocal microscope.

In previous works it was shown that the morphology of the structures strongly depends on the growth process. Thermal treatments at 1150 °C of metallic gallium on gallium oxide pellets lead to the formation of undoped nanowires and microstructures as it has been previously reported.[12,13] A representative secondary electron image is shown in Figure 1a. To dope the micro- and nanostructures, indium oxide powders were placed along with Ga onto the substrate, and a double-step thermal treatment has been used as described above. SEM images of planar microstructures, nanobelts, and springs are shown in parts b−f of Figure 1. The presence of In appears to favor the formation of belts which are only occasionally observed in the case of undoped structures. Also, a characteristic of the In-doped samples is that some of the belts are twisted leading to springs with sawlike edges (parts d and e of Figure 1). Other planar structures of variable thickness seem to be formed with some well-defined steps on the microstructure surface (figure 1f). Figure 2 shows the XRD spectrum of the
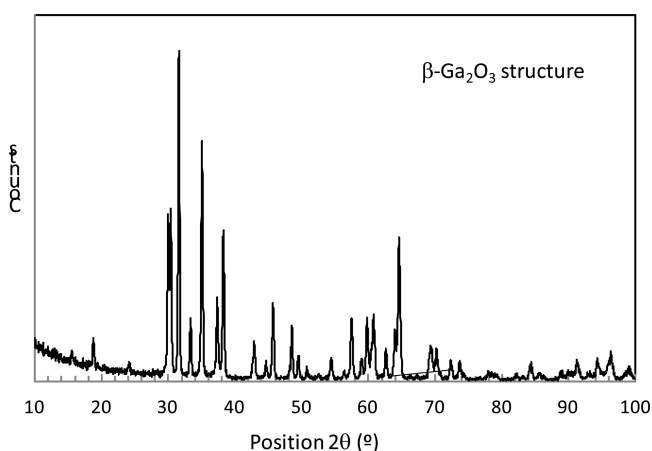
Figure 2. XRD spectrum of the obtained indium-doped Ga_2O_3 micro- and nanostructures. Peaks maxima correspond to monoclinic β-Ga_2O_3 phase.

obtained structures. All diffraction peaks can be indexed to a monoclinic gallium oxide (β-Ga_2O_3) crystal structure, $C2/m$ space group, and reticular parameters of a (Å) = 12,227, b (Å) = 3,039, c (Å) = 5,808, being α = 90°, β = 103.82°, and γ=90° (JCPDS 00−041−1103). No additional peaks related to an eventual formation of an indium oxide phase during the growth process were detected.

TEM images (parts a and b of Figure 3) show the morphology of some of the structures observed by SEM with stepped borders (Figure 1e). The structure shown in figure 3 has an average width under 100 nm and a nanoherringbone appearance related to twin defects, which could be involved in the growth process and be responsible for the final morphology. Figure 3c shows the corresponding HRTEM image at higher magnification and the SAED pattern along the [100] zone axis, where streaking of the main diffraction spots
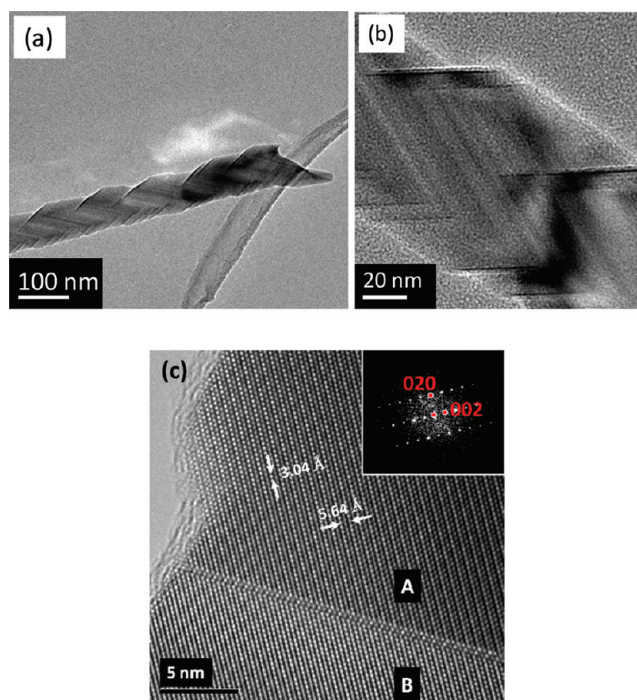

Figure 3. (a) and (b) TEM images of In-doped Ga_2O_3 nanostructures showing lateral zigzag contour. (c) HRTEM image and SAED pattern along the [100] zone axis, where streaking of the main diffraction spots along the (011) direction can be observed.

along the (011) direction can be observed. This fact is a signature of structural disorder and is due to the presence of recurrent twinning. We have calculated as well fast Fourier Transform (FFT) patterns in different domains of the nanoherringbone marked as A and B in Figure 3c. The results show identical patterns with no extra spots, hence no additional order is observed and identical crystalline structure retains in the whole nanostructure. The measured interplanar distances are 0.304 and 0.564 nm, which fit well to the b and c parameters of the β-Ga_2O_3 unit cell, respectively. In addition, EDS microanalysis shows an In content of about 5 at % and that the average Ga and In atoms distribution on both sides of the twin plane is homogeneous, which verifies that this disorder is not related to chemical composition variations at this nanoscale. Furthermore, it is worth mentioning that the electron beam focus is different in regions marked A and B, which suggests that an extra layer is introduced on an upper plane leading to a step, probably as a consequence of the crystal growth process.[14] Linear and planar defects may play a crucial role in the nucleation and growth of one-dimensional structures. For example, axial screw dislocations provide self-perpetuating steps leading to hierarchical nanostructure in ZnO nanowires on GaN substrates.[15,16] Another example is the layer-by-layer model proposed for the growth of Ga_2O_3 nanobelts formed by two single crystalline nanowires, with a twin boundary along the longitudinal axis.[17,18] Our TEM and HRTEM observations show the presence of In into the single crystalline β-Ga_2O_3 structures and that twinning is generated during the growth process of the In-doped Ga_2O_3 nanostructures.

To study the effect of the chemical composition on the luminescence properties of Ga_2O_3 we have performed correlative EDS and CL measurements of these structures in the SEM. Indium-doped structures were placed and fixed onto

a silicon wafer. The appearance of terraces and steps on the planar surfaces usually led to a zigzag edge. Parts a and b of Figure 4 show the secondary electron image and the
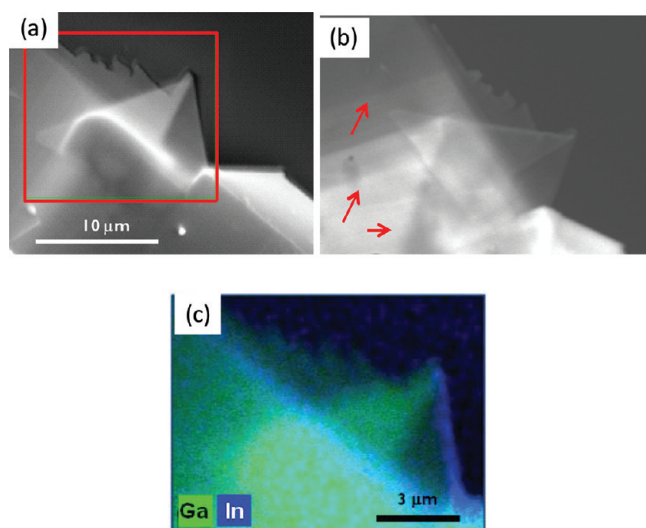

Figure 4. (a) SEM image, (b) CL image, and (c) X-ray microanalysis mapping of the same area.

corresponding CL panchromatic image of one of the structures. The CL image shows some features in the microstructure (marked with arrows in Figure 4b), not observed in the SE image. The origin of the contrast in a CL image is often related to the defect structure in the sample. Oxygen vacancies are native defects in Ga_2O_3 responsible for a broad luminescence band in the ultraviolet-blue region.[19,20] The observed contrast in the CL image suggests that defects are mainly distributed along terraces and steps of the microstructure. Ga and In X-ray microanalysis mapping of the same region is shown in figure 4c. Green color stands for Ga atoms while blue color for In ones. The image clearly shows accumulation of In atoms at certain lateral edges, which reveals impurity segregation during the growth process. Table I shows the indium concentration

Table I. EDX Data at Selected Points in Figure 5a

selected point	In at % (EDX)
A (outer)	6
B	5
C	3
D (inner)	1

obtained from the quantitative analysis of the EDX spectra from selected points in a different edge of the microstructure shown in Figure 4 (Figure 5a). These values range from 1 at % (D point) to 6 at % (A point), which correspond to inner and outer points, respectively. Local CL spectra recorded at these points are shown in Figure 5b. Blue UV emission bands have been reported in the literature for gallium oxide, and several component—2.7, 3.1, and 3.4 eV—were identified. The origin of these emissions was assigned to self-trapped excitons (UV component) and donor−acceptor pair transitions (blue band). Donors are related to oxygen vacancies or Ga interstitials, and oxygen−gallium vacancies pairs were supposed to be the acceptor centers.[20,21] The incorporation of impurities may modify the defect levels inducing luminescence changes. In our

| selected point	In % (EDX)
A	6
B	5
C	3
D	1
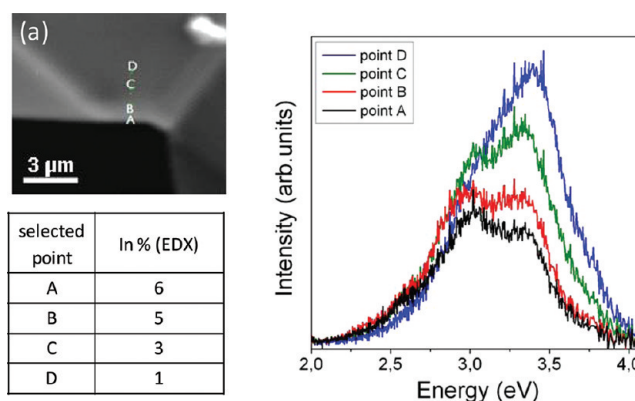
Figure 5. (a) SEM image of a microstructure. (b) CL spectra recorded from points A, B, C, and D marked in (a). Table shows data of In concentration for the marked points in (a).

case, the incorporation of In results in the relative decrease of the UV component with respect to the blue one as we go toward the structure edge (from D point to A point). This is related to the variations in In concentration detected by EDS so that the higher the indium content, the stronger is the blue (2.7 − 3.0 eV) component as shown in the CL spectrum at point A (Figure 5b), while for lower In concentration, the main CL emission corresponds to the UV band (3.4 eV), approaching the result obtained for undoped Ga_2O_3 samples.[20] This behavior shows that In atoms are strongly involved in the blue component (DAP transition), possibly by interaction with oxygen vacancies. As these native defects supply free carriers for conduction and introduce electronic energy levels in the band gap, the blue shift in CL spectra as indium concentration increases (EDS spectra) is quite relevant for potential optoelectronic devices based on In-doped Ga_2O_3 structures. Therefore, both optical and electronic properties could be tunable by modification of defect structure by In doping.

These results can be related to the growth and doping processes where In impurities and twin boundaries play a relevant role. The contrast observed in CL images show parallel fringes probably originated as a consequence of a nonuniform In concentration in the microstructures. These fringes seem to end in fronts where In atoms are accumulated as EDS data show. To explain the reason of the In segregation following parallel fronts we have to get insight into the growth and doping process. The role of twins may be relevant to explain the final morphology, as TEM results show. Planar defects are preferential places where impurities and point defects accumulate. The growth process involves indium incorporation into gallium oxide microstructures, which exhibit twin defects. Therefore, In atoms would accumulate during the growth at the twin plane, and the layer-by-layer process would result in the formation of steps and terraces, which would explain the bright stripes observed in CL images.

Additional relevant information of the local microstructure of In-doped Ga_2O_3 has been obtained by means of XPS and Raman measurements performed on In-doped and on undoped Ga_2O_3 structures. XPS spectra for Ga 3d and O 1s in undoped Ga_2O_3 nanostructures obtained with the same procedure as the In-doped ones are shown in Figure 6. Energy axis was calibrated by fixing C 1s binding energy (BE) at 284.8 eV.[22] There is a general agreement in the literature to assign 20.6 eV as binding energy of Ga^{3+} in Ga_2O_3. For example, the NIST database gives a value of 20.4 ± 0.5 eV for Ga 3d $^{5}/_{2}$ in

3938

dx.doi.org/10.1021/jp210233p | J. Phys. Chem. C 2012, 116, 3935−3943
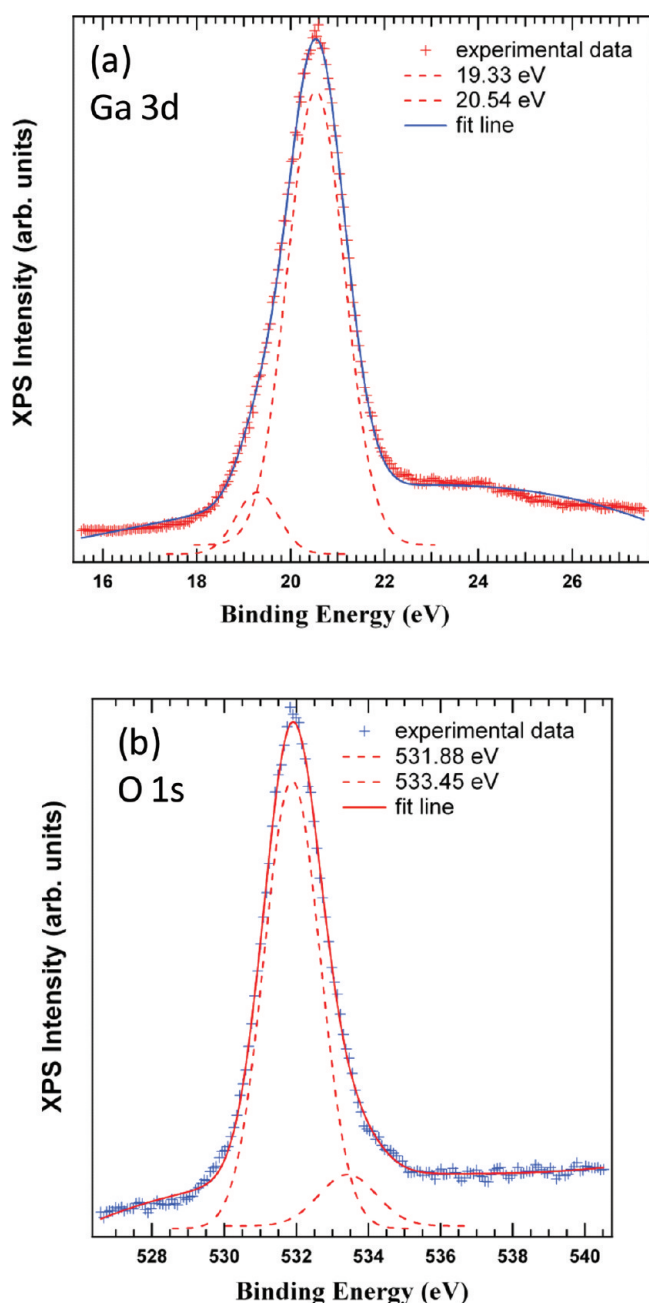
Figure 6. XPS high resolution spectra of Ga 3d (a) and O 1s (b) lines in undoped Ga_2O_3 microstructures.

Ga_2O_3.[23] Ghosh et al. have measured the XPS spectra for Ga_2O_3 standard,[24] and peaks at 20.07 and 20.52 eV were assigned to Ga 3d, while small amounts of an unidentified impurity (possibly metallic gallium) gave rise in the fitting process to peaks at 19.28 or 18.84 eV. The main peak in Figure 6a, at 20.54 eV for the Ga 3d core level, corresponds to Ga^{3+} in the Ga−O bonding, and the lower energy shoulder at 19.33 eV could be related to a small amount of metallic Ga or Ga suboxide at the surface. Figure 6b shows the XPS spectrum of the O 1s core level. Experimental data can be fitted to the sum of two Gaussians with maxima at 531.88 and 533.45 eV, respectively. These values are also consistent with those reported for Ga_2O_3 standard in the literature.[25] For metal oxides, the lower BE component is usually assigned to the oxide (i.e., Ga−O−Ga bonds). The higher BE component is usually

assigned to the hydroxide (OH)/adsorbed oxygen $(O_2)^{2-}$ species and may have contributions from adsorbed water.[26] XPS images recorded with the Ga 3d, O 1s, or C 1s binding energies reveal mainly topographic contrast and no significantly local changes of XPS spectra are observed in the images.

Therefore, from the chemical point of view, the composition of the undoped Ga_2O_3 nanostructures is quite uniform, and the oxidation process of the metallic gallium was completed during the growth. The binding energies for Ga 3d and O 1s peaks in undoped Ga_2O_3 nanostructures will be used for comparison with the corresponding core levels in the In-doped ones. A survey spectrum of In-doped Ga_2O_3 nanostructures (not shown) shows peaks related to core levels of O 1s (531.8 eV), In 3d (453.07 and 445.85 eV), C 1s (284.8 eV), Ga 3p (106.7 eV), and Ga 3d (20.1 eV), along with O Auger peaks. Figure 7a displays an XPS image recorded with the In 3d binding energy of the In-doped microstructure shown in Figure 4. High-resolution XPS spectra of the O 1s and Ga 3d lines have been recorded from the two points marked in Figure 7a, at different distances from the edge. EDS measurements performed in the SEM from these points yielded a composition of 2.7 at % at A point and 1.0 at % at B point. The analysis of XPS spectra (not shown) of the Ga 3d line from both A and B points gives two components listed in Table II. The obtained values are very close to each other, and the XPS image with the Ga 3d energy is quite uniform both for undoped and for In-doped samples. The only feature observed is a slight shift of the components toward higher binding energies at point B (1 at % In) with respect to point A or undoped Ga_2O_3. Let us now consider the XPS spectra of the O 1s core level in undoped and doped Ga_2O_3 microstructures shown in parts b and c of Figure 7. Table III summarizes the data obtained after the fitting process for O 1s line. As it can be seen, the number of components needed to get a good fit varies in each sample or position.

At point A, corresponding to higher In incorporation (2.7 at % In), the main component related to Ga−O bonds at 531.87 eV and the higher binding energy component at 533.24 eV are clearly similar to those of undoped samples. In addition, a lower binding energy component (530.02 eV), which could be related to In−O bonds appears as a shoulder in the XPS spectra. The binding energy of O 1s core level for In_2O_3 is 530.2 eV, as reported in ref 25. As it has been mentioned above, indium tends to occupy gallium lattice sites in the gallium oxide lattice. As both elements participate in the bonding with the same charge state, it is expected that O 1s core levels characteristic of Ga_2O_3 and In_2O_3 may appear in the XPS spectra, as it occurs at point A (530.02 eV for In−O and 531.87 eV for Ga−O) close to the edge. On the other hand, at point B (1.0 at % In), only one component is detected in the XPS spectrum at 532.03 eV, which may be attributed to Ga−O bonds. These results indicate that the O 1s core levels are the most affected by In doping in Ga_2O_3. Also, In 3d lines have been measured, and the same values (445.59 and 453.42 eV) at both A and B points were obtained (Figure 7d). This binding energy agrees with the In^{3+} state in In_2O_3 (445.1 eV).[21] XPS measurements performed in In-doped Ga_2O_3 nanobelts and springs yielded similar results. For example, Figure 8a shows the XPS mapping recorded with the Ga 3d energy line in a springlike structure. High-resolution O 1s XPS spectra of the points marked as B and C in the inset of Figure 8a are shown in Figure 8b. Only the component at 531.7 eV is observed (Ga−O bonding in Ga_2O_3) at B point, while a shoulder at lower binding energies is clearly resolved
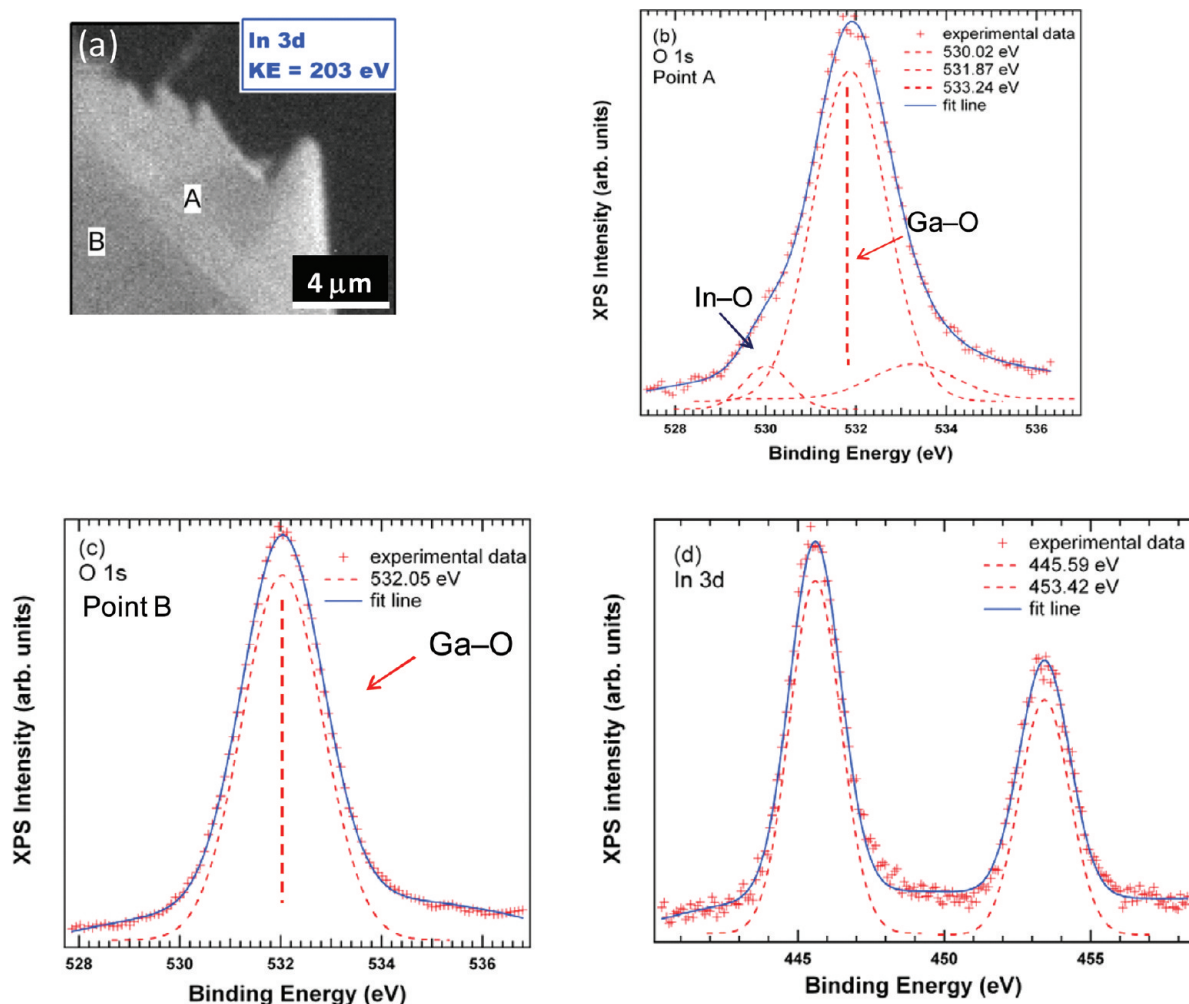
Figure 7. (a) XPS mapping recorded with the In binding energy. (b and c) High-resolution XPS spectra of O 1s lines from A and B points marked in (a), respectively. (d) XPS spectra of In 3d lines in In-doped Ga_2O_3 microstructure.

Table II. Binding Energies (in eV) of the Ga 3d Core Level in Undoped and In-Doped Samples

undoped	In-doped, point A	In-doped, point B
19.33	19.20	19.53
20.54	**20.55**	**20.61**

Table III. Binding Energies (in eV) of the O 1s Core Level in Undoped and In-Doped Samples

| undoped	In-doped, point A	In-doped, point B
	530.02	
531.88	**531.87**	**532.03**
533.45	533.24	

(529.6 eV) and related to the In–O bond at C point. The analysis of high resolution XPS core level spectra of Ga 3d, O 1s, and In 3d enable to determine the oxidation degree of gallium oxide structures and the effectiveness of indium incorporation into this matrix at the chemical bonding level.

The influence of the indium concentration on the vibrational spectrum of the samples has been characterized by spatially resolved Raman spectroscopy in a confocal microscope. Figure 9a shows the Raman spectrum of an undoped β-Ga_2O_3 nanoribbon obtained by the same thermal treatment as the In-doped ones. The spectrum is similar to those reported for bulk material,[27,28] and shows the characteristic peaks at 200, 346, 416, 475, 627, 657, and 765 cm^{-1}. The peak at 520 cm^{-1} corresponds to the silicon substrate. Figure 9b shows a comparison of the different Raman peaks acquired from two points of the β-Ga_2O_3:In microstructure shown in Figures 4 and 7, where In concentration was 1 and 6 at %, respectively. The peaks from the undoped structure (Figure 9a) are also added for comparison. A different evolution of the peaks is observed when increasing the In concentration. In the case of 1 at % In concentration, virtually no changes are observed with respect to the undoped sample, except for a light increase of the 651 cm^{-1} peak intensity, as explained below. For 6 at % In concentration, the 200, 320, and 765 cm^{-1} peaks do not change while a slight broadening of the 345 and 470 cm^{-1} peaks and a stronger, asymmetric widening of the 415 and 630 cm^{-1} peaks takes place. Finally, a clear increase of the intensity ratio of the 651 cm^{-1} (A_g) and 657 cm^{-1} (B_g) with increasing In content is observed.

The β-Ga_2O_3 crystal structure consists of a double chain of GaO_6 octahedra, which is connected by GaO_4 tetrahedra.[29] Hence, there are two nonequivalent Ga^{3+} sites in the β-Ga_2O_3 lattice: Ga_I (tetrahedral coordination) and Ga_{II} (octahedral coordination and longer bond lengths). Dohy et al.[28] performed a theoretical and experimental vibrational study of the bulk β-Ga_2O_3 structure, which resulted in 15 Raman-active
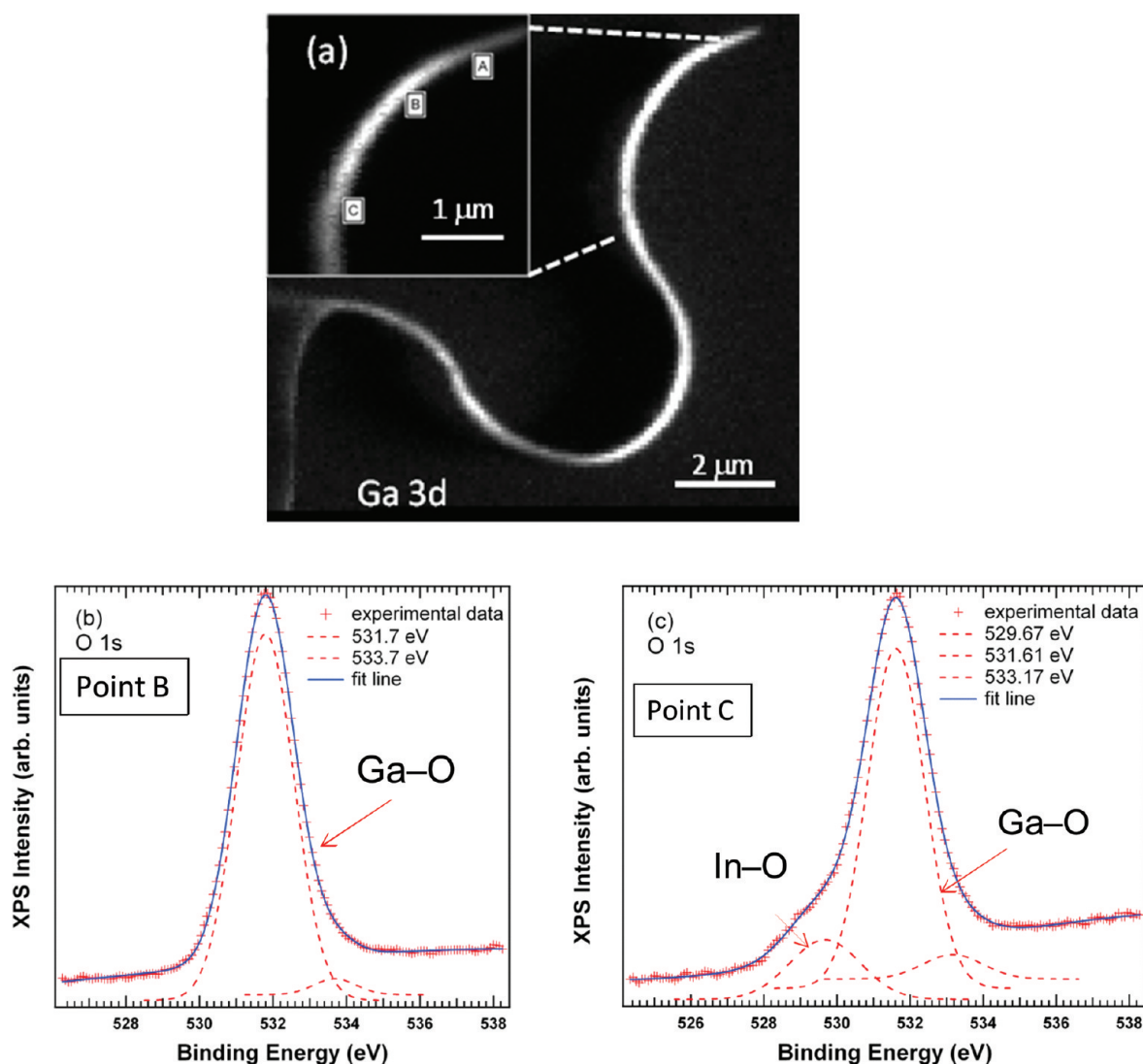
Figure 8. (a) XPS mapping with Ga 3d binding energy of an springlike structure. Inset detail at high magnification with some points marked. (b and c) High-resolution XPS spectra of O 1s lines from B and C points, respectively.

modes. The Raman spectrum was divided in three regions accordingly with the frequency peaks range: low-frequency peaks (up to 200 cm^{-1}), high-frequency peaks (above ~600 cm^{-1}), and an intermediate range between 300 and 600 cm^{-1}. These ranges were related to different vibration modes. However, they observed that vibrations seem to be heavily mixed.[28] It is well-known that impurities which are heavier than the host atoms create nonlocal modes coupled to the host continuum which results in a broadening of Raman lines.[30] It has been shown that, in β-(Ga$_{1-x}$In$_x$)$_2$O$_3$ solid solutions with low indium concentrations, In^{3+} ions are preferentially located in the octahedral sites,[31,32] which would imply variations in the intermediate frequency range of Raman spectra. Within this framework, the lines width increase observed in this work, stronger for 345, 417, 470, and 630 cm^{-1}, should be related to the influence of the In^{3+} located in the Ga$_{II}$ octahedral site on these Raman modes. This effect is clearly observed in the Raman spectra recorded at points in the structure with higher In content.

On the other hand, the most noticeable effect observed in the Raman spectra of In-doped Ga$_2$O$_3$ is the enhancement of the relative intensities of the 651/657 cm^{-1} peaks, even at

points with a lower In content. The 657 cm^{-1} peak was reported by some authors as a single peak[33−35] in bulk and Ga$_2$O$_3$ nanorods, although a composed peak (651−654 cm^{-1}) was also reported in bulk Ga$_2$O$_3$[28] and in Ga$_2$O$_3$−In$_2$O$_3$ solid solutions.[36] We have observed that the main component in undoped samples is the 657 cm^{-1} peak, while the 651 cm^{-1} one dominates in the In-doped region. The variation in phonon spectra due to doping or size effects could be relevant as it may affect to the heat transfer and electron−phonon interactions. Thermal management in electronic devices is of practical importance and optical phonons are usually involved in electrical and optical properties.

In summary, In-doped Ga$_2$O$_3$ micro- and nanostructures, with different morphology including nanoribbons and nano-springs, have been grown by thermal oxidation of Ga. Indium incorporation in the range 1−6 at % has been detected by several spectroscopic tools used in this work (EDS in HRTEM, EDS in SEM, and XPS). The novel morphologies, such as springs and belts with jagged edges, can be explained by taking into account the presence of twins in the crystals (HRTEM analysis). The layer-by-layer model proposed as growth mechanism is consistent with the appearance of terraces and
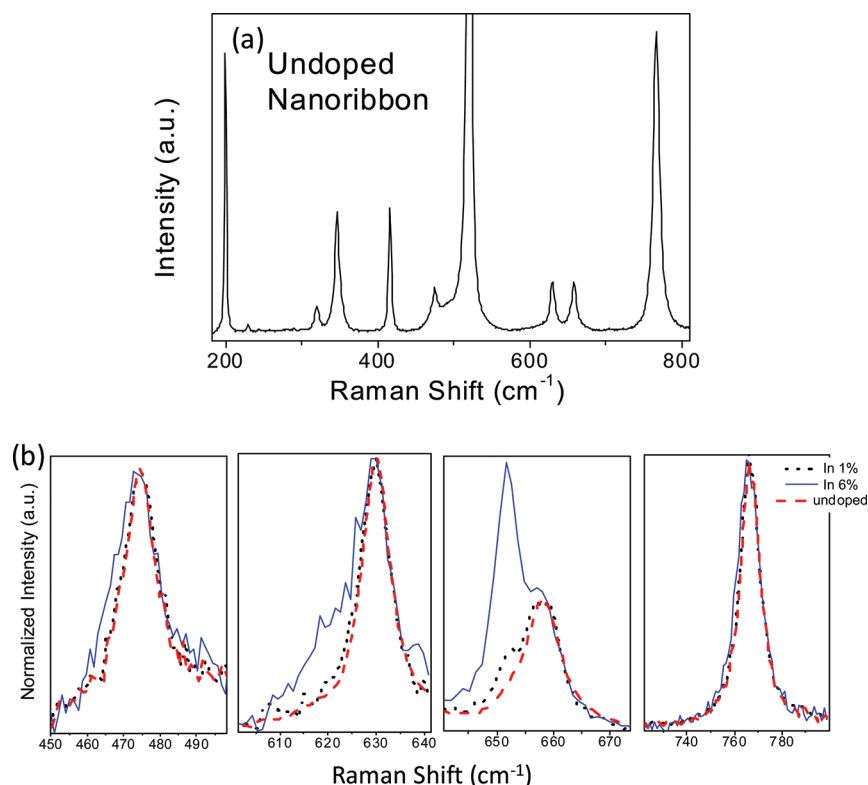
Figure 9. (a) Micro-Raman spectrum of undoped gallium oxide nanostructure where characteristic peaks of Ga_2O_3 are shown. The peak at 520 cm^{-1} corresponds to the silicon substrate. (b) Detailed Raman spectra showing the evolution of peaks at 651 and 657 cm^{-1} from undoped (dashed line), In 1 at % (dashed line) and In 6 at % (solid line).

steps in the planar surfaces. Moreover, a segregation of In impurities at the edges suggests that In may influence the growth mechanism. In incorporation modifies the native defect structure as observed by means of local CL spectra recorded at several points in the doped nanostructures. A blue, defect-related luminescence band is found to strongly increase when increasing the In content. The inclusion of In ions in the octahedral Ga sites does not result in a strong modification of the vibrational modes of the crystal up to 6 at % In, as observed by spatially resolved Raman spectroscopy, with exception of an intensity increase of the 651 cm^{-1} A_g mode and broadening of some peaks.

■ AUTHOR INFORMATION

Corresponding Author
*E-mail: bianchi@fis.ucm.es.

Notes
The authors declare no competing financial interest.

■ REFERENCES

(1) Ginley, D. S.; Bright, C. *MRS Bull.* **2000**, *25*, 15.
(2) Dai, Z. R.; Pan, Z. W.; Wang, Z. L. *Adv. Funct. Mater.* **2003**, *13*, 9.
(3) Yamaga, M.; Víllora, E. G.; Shimamura, K.; Ichinose, N.; Honda, M. *Phys. Rev. B* **2003**, *68*, 155207.
(4) Varley, J. B.; Weber, J. R.; Janotti, A.; Van de Walle, C. G. *Appl. Phys. Lett.* **2010**, *97*, 142106.
(5) Víllora, E. G.; Shimamura, K.; Yoshikawa, Y.; Ujiie, Y.; Aoki, K. *Appl. Phys. Lett.* **2008**, *92*, 202120.
(6) Chiang, H. Q.; Hong, D.; Hung, C. M.; Presley, R. E.; Wager, J. F.; Park, C. H.; Keszler, D. A.; Herman, G. S. *J. Vac. Sci. Technol. B.* **2006**, *24*, 2702.
(7) Lu, J. G.; Chang, P.; Fan, Z. *Mat. Sci. Eng. R* **2006**, *52*, 49.
(8) Hidalgo, P.; Liberti, E.; Rodríguez-Lazcano, Y.; Méndez, B.; Piqueras, J. *J. Phys. Chem. C* **2009**, *113*, 17200.
(9) Nogales, E.; García, J. A.; Méndez, B.; Piqueras, J. *Appl. Phys. Lett.* **2007**, *91*, 133108.
(10) Nogales, E; Hidalgo, P; Lorenz, K; Méndez, B; Piqueras, J; Alves, E *Nanotechnology* **2011**, *22*, 285706.
(11) Mazeina, L.; Piccard, Y. N.; Maximenko, S. I.; Perkins, F. K.; Glaser, E. R.; Twigg, M. E.; Freitas, J. A.; Prokes, S. M. *Cryst. Growth Des.* **2009**, *9*, 4471.
(12) Nogales, E.; Méndez, B.; Piqueras, J.; García, J. A. *Nanotechnology* **2009**, *20*, 115201.
(13) Nogales, E.; Méndez, B.; Piqueras, J. *Ultramicroscopy* **2011**, *111*, 1037.
(14) van de Waal, B. W. *J. Cryst. Growth* **1996**, *158*, 153.
(15) Jin, S.; Bierman, M. J.; Morin, S. A. *J. Phys. Chem. Lett.* **2010**, *1*, 1472.
(16) Morin, S. A.; Jin, S. *Nano Lett.* **2010**, *10*, 3459.
(17) Kim, H. W.; Shim, S. H. *Thin Solid Films* **2007**, *515*, 5158.
(18) Jalilian, R.; Yazpanah, M. M.; Pradhan, B. K.; Sumanasekera, G. U. *Chem. Phys. Lett.* **2006**, *426*, 393.
(19) Binet, L.; Gourier, D. *J. Phys. Chem. Solids* **1998**, *59*, 1241.
(20) Díaz, J.; López, I.; Nogales, E.; Méndez, B.; Piqueras, J. *J. Nanoparticle Res* **2011**, *13*, 1833.
(21) Shimamura, K.; Víllora, E. G.; Ujiie, T.; Aoki, K. *Appl. Phys. Lett.* **2008**, *92*, 201914.
(22) Miller, D. J.; Biesinger, M. C.; McIntyre, N. S. *Surf. Interface Anal.* **2002**, *33*, 299.

3942

dx.doi.org/10.1021/jp210233p | *J. Phys. Chem. C* 2012, 116, 3935−3943

(23) http://srdata.nist.gov/xps

(24) Ghosh, S. C.; Biesinger, M. C.; LaPierre, R. R.; Kruse, P. *J. Appl. Phys.* **2007**, *101*, 114322.

(25) Hollinger, G.; Skheyta-Kabbani, R.; Gendry, M. *Phys. Rev. B* **1994**, *49*, 11159.

(26) Al-Kuhaili, M. F.; Durrani, S. M. A.; Khawaja, E. E. *App. Phys. Lett.* **2003**, *83*, 4533.

(27) Li, Y.; Liu.; Lee, C. S.; Lee, S. T. *Superlattices Microstruct.* **2009**, *46*, 585.

(28) Dohy, D.; Lucazeau, G.; Revcolevschi, A. *J. Solid State Chem.* **1982**, *45*, 180.

(29) Kudo, A.; Mikami, I. *J. Chem Soc., Faraday Trans* **1998**, *94*, 2929.

(30) *Raman scattering in materials science*; Weber, W. H., Merlin, R., Eds.; Springer, 2010.

(31) Edwards, D. D.; Folkins, P. E.; Mason, T. O. *J. Am. Ceram. Soc.* **1997**, *80*, 253.

(32) Blanco, M. A.; Sahariah, M. B.; Jiang, H.; Costales, A.; Pandey, R. *Phys. Rev. B* **2005**, *71*, 184103.

(33) Gao, Y. H.; Bando, Y.; Sato, T.; Zhang, Y. F.; Gao, X. Q. *Appl. Phys. Lett.* **2002**, *81*, 2267.

(34) Rao, R.; Rao, A. M.; Xu, B.; Dong, J.; Sharma, S.; Sunkara, M. K. *J. Appl. Phys.* **2005**, *98*, 094312.

(35) Zhao, Y.; Frost, R. L. *J. Raman Spectrosc.* **2008**, *39*, 1494.

(36) Vigreux, C.; Binet, L.; Gourier, D. *J. Solid State Chem.* **2001**, *157*, 94.